

Discovering topological phases in gray-Tin

Gaurav Harsha,¹ Selina Dirnböck,^{2,3} Emanuel Gull,^{2,4} Vojtěch Vlček,^{5,6} and Dominika Zgid^{1,2,4}

¹*Department of Chemistry, University of Michigan, Ann Arbor, MI 48109, USA*

²*Department of Physics, University of Michigan, Ann Arbor, MI 48109, USA*

³*Institute of Solid State Physics, TU Wien, 1040 Vienna, Austria*

⁴*Department of Physics, University of Warsaw, Pasteura 1, 02-093 Warsaw, Poland*

⁵*Department of Chemistry and Biochemistry, University of California, Santa Barbara, CA 93106, USA*

⁶*Department of Materials, University of California, Santa Barbara, CA 93106, USA*

(Dated: December 1, 2025)

Non-trivial topological phases often emerge in narrow-gap semiconductors with a delicate blend of spin-orbit coupling and electron correlation. The diamond-lattice allotrope of Sn (α -Sn) exemplifies this behavior, hosting multiple topological phases that can be tuned by small distortions in the lattice. Despite rapid experimental progress, theoretical descriptions of α -Sn lack predictive power and rely mainly on tight-binding models and density functional theory with uncontrolled approximations. We employ first-principles fully self-consistent, relativistic *GW* (sc*GW*) to overcome these limitations. The sc*GW* recovers the experimentally observed zero-gap semiconductor and the strain-induced topological insulator and Dirac semimetal phases, while also predicting new trivial and topological insulators and a Dirac semimetal phase, further demonstrating the versatility of α -Sn for band engineering. Additionally, we propose a robust diagnostic of topological behavior based on a combined analysis of band and orbital-occupation dispersions, tailored for correlated methods where standard mean-field-based topological invariants fall short. Our findings pave the way for studying a broad class of topological materials using accurate first-principles methods beyond density functional theory.

INTRODUCTION

Gray-tin (α -Sn), an allotrope of tin with a diamond lattice, hosts a variety of topological phases. While its ground state is a zero-gap semimetal [1], small uniaxial strains can drive the material into topologically non-trivial phases, including a three-dimensional topological Dirac semimetal (3D-TDS) and a topological insulator (TI) [2–13]. Thin films of α -Sn are generally deposited on substrates such as InSb [3–5, 7, 8, 10] or CdTe [2, 6, 11–13]. By controlling substrate orientation and lattice mismatch, different types of uniaxial strain, and thus distinct topological phases, can be induced. Notably, an in-plane compressive strain of less than 1% along the [111] plane (in the conventional cubic unit cell) drives the formation of a 3D TDS phase [3, 7, 11, 12], whereas compression along [001] results in a TI [4, 8, 10, 14] or 3D TDS depending on film thickness. The strong interplay among electron correlation, relativity and lattice distortions results in a highly tunable electronic structure, making α -Sn an appealing platform for practical applications[15–20].

Theoretical investigations of α -Sn [3, 12, 21–24] have relied primarily on density functional theory (DFT), often as a descriptive tool to complement experiments. In many cases, parameters in the exchange-correlation functional are adjusted to reproduce specific features observed in experiments [3, 12], such as the Γ -point band dispersion observed in angle-resolved photo-emission spectroscopy (ARPES). Prediction of band inversions in bulk α -Sn has also proved difficult within DFT [24].

This challenge extends beyond α -Sn. For small band-gap materials designed as candidates for TIs, theoretic-

cal predictions are indispensable, since experiments frequently provide an incomplete picture. ARPES probes only the occupied bands, while complementary techniques such as inverse photoemission [25] and time-resolved ARPES [26] suffer from noise, non-equilibrium effects, and other technical limitations. Likewise, transport measurements can be obscured by impurities and substrate effects. Therefore, accurate insights from theory are crucial to fully interpret topological character in a material.

Topological band theory [27–29] provides techniques to analyze mean-field and DFT results, offering valuable qualitative insights into the emergence of topological phases, particularly in weakly correlated systems [30–34]. However, for topological materials where narrow band gaps are modulated by electronic correlations, DFT develops a strong dependence on exchange-correlation functions, and often leads to contradictory predictions [35, 36]. Advanced many-body approaches beyond DFT are essential for unraveling the rich phase diagram of correlated topological materials [37–41].

In this article, we employ *ab-initio* fully self-consistent *GW* (sc*GW*) [42–45] to provide a reliable interpretation of experimental observations for α -Sn. In particular, we focus on the variation in band structure as a function of both uniform and anisotropic strain. The *GW* method accurately captures electron-electron correlation through orbital-selective screened Coulomb interactions, especially in systems where correlation is governed by density fluctuations. By including both scalar-relativistic effects and spin-orbit coupling (SOC) within the exact two-component (X2C) framework [46–50], our

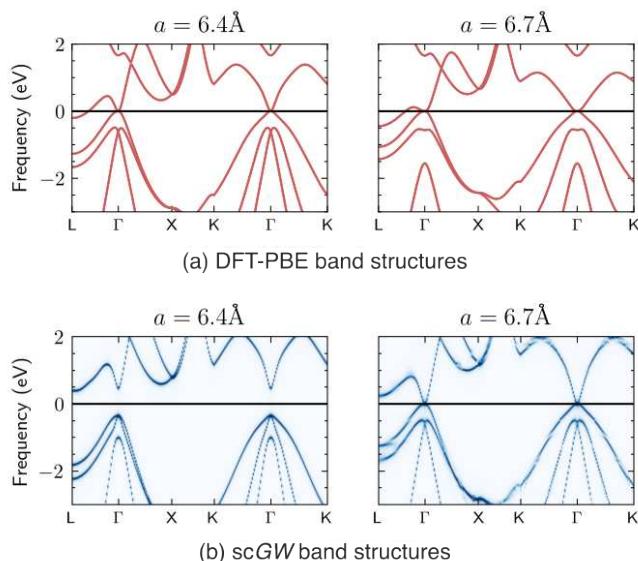


FIG. 1. (a) PBE and (b) scGW Band structures for α -Sn for lattice constants ranging $a = 6.4$ and 6.7 Å along the L - Γ - X - K - Γ - K high-symmetry path.

GW implementation [51–54] captures the distinct topological phases observed in α -Sn. Moreover, enforcing full self-consistency eliminates any dependence on the choice of DFT functional, overcoming the pitfalls of one-shot and partially self-consistent approaches [36, 55]. In what follows, we use scGW to denote the relativistic X2C-based scGW framework.

RESULTS

We first compare the DFT and scGW band structures of α -Sn across a wide range of lattice parameters. The self-consistent GW predicts an equilibrium lattice constant of $a \simeq 6.45$ Å, whereas DFT estimates vary between 6.45 – 6.67 Å depending on the functional [22, 56]; the experimental value is 6.49 Å [57, 58]. Given this spread, we analyze lattice constants in the range $a = 6.4$ – 6.7 Å. For DFT calculations, we use the Perdew-Burke-Ernzerhof (PBE) exchange-correlation functional [59] as a representative choice.

Figure 1 compares PBE and scGW band structures at $a = 6.4$ Å and $a = 6.7$ Å. In both cases, PBE predicts a negative band gap with conduction band minima at L lying below the valence band maximum at Γ , contradicting experimental observations [2]. This deficiency persists across other DFT functionals [22, 23]. By contrast, scGW restores the correct band ordering throughout the Brillouin zone and yields a zero gap at Γ for $a = 6.7$ Å, consistent with experiments [1, 2].

Figure 2(a)-(b) show the evolution of the band structure along K - Γ - X for several lattice constants. PBE in-

variably predicts a zero gap at Γ and a negative Γ - L gap across all lattices. To the contrary, scGW results display a sensitive lattice-dependent evolution. For $a = 6.7$ Å, scGW predicts a zero gap semimetal with an M-shaped band, in agreement with ARPES [10]. As the lattice is compressed, the $5s$ and $5p$ orbital occupations at Γ exhibit a sharp change (Fig 2(c)), indicating a pronounced reordering of the bands. Also captured in orbital-resolved band dispersions (Fig. 1 of SI), this reordering manifests as a sequence of distinct phases, schematically depicted in Fig. 2(d). At $a = 6.7$ Å, SOC pushes the $5s$ valence band below the $5p$ bands, producing a double inversion in orbital ordering and giving rise to topological surface states [4, 10]. At smaller lattice constants ($a \leq 6.5$ Å), SOC effects are suppressed, and the $5s$ orbital shifts entirely above the Fermi level, opening a trivial band gap and yielding a semiconductor. At the phase boundary ($a \simeq 6.55$ – 6.6 Å), the renormalized $5s$ bands result in linearly dispersing Dirac cones at the Fermi level, forming a three dimensional Dirac semimetal. While such Dirac semimetals are known in other materials [60–62], experimental validation for α -Sn requires further investigation.

The evolution of the four-fold degeneracy in the valence bands further highlights the qualitative changes in electronic structure. At $a = 6.7$ Å, the degeneracy occurs at the Fermi level due to the touching of doubly degenerate valence and conduction bands. In contrast, at $a = 6.4$ Å, the re-ordered four-fold degeneracy arises from two doubly degenerate valence bands, marking a clear transition to a trivial insulating state. Together, the orbital-resolved occupations and band dispersions provide a consistent picture of the lattice-driven evolution from a semimetal through a Dirac semimetal to a trivial insulator.

Unlike mean-field approaches, where topological invariants and surface states can be readily computed using established tools [63, 64], correlated methods lack such straightforward diagnostics. Consequently, phase identification often relies on indirect evidence, such as detailed comparisons of band dispersions and orbital characters between trivial and non-trivial phases [65]. Here, we analyze orbital-resolved bands and occupation trends in the symmetrized atomic orbital (SAO) basis to trace the evolution of band topology. We note that alternative approaches based on Green’s-function zeros are also being actively explored [66–68], though their applicability to first-principles calculations remains unclear.

We now analyze the effect of uniaxial strain in α -Sn. Figure 3 shows the scGW band structures under compressive and tensile strain perpendicular to $[001]$, i.e., along the c -axis. These configurations are equivalent to in-plane stretching and compression along $[001]$, respectively, as typically realized in practical setups. We use $a = 6.7$ Å as the reference lattice constant for the strained structures. While this value is slightly smaller than experiment, the resulting unstrained band structure

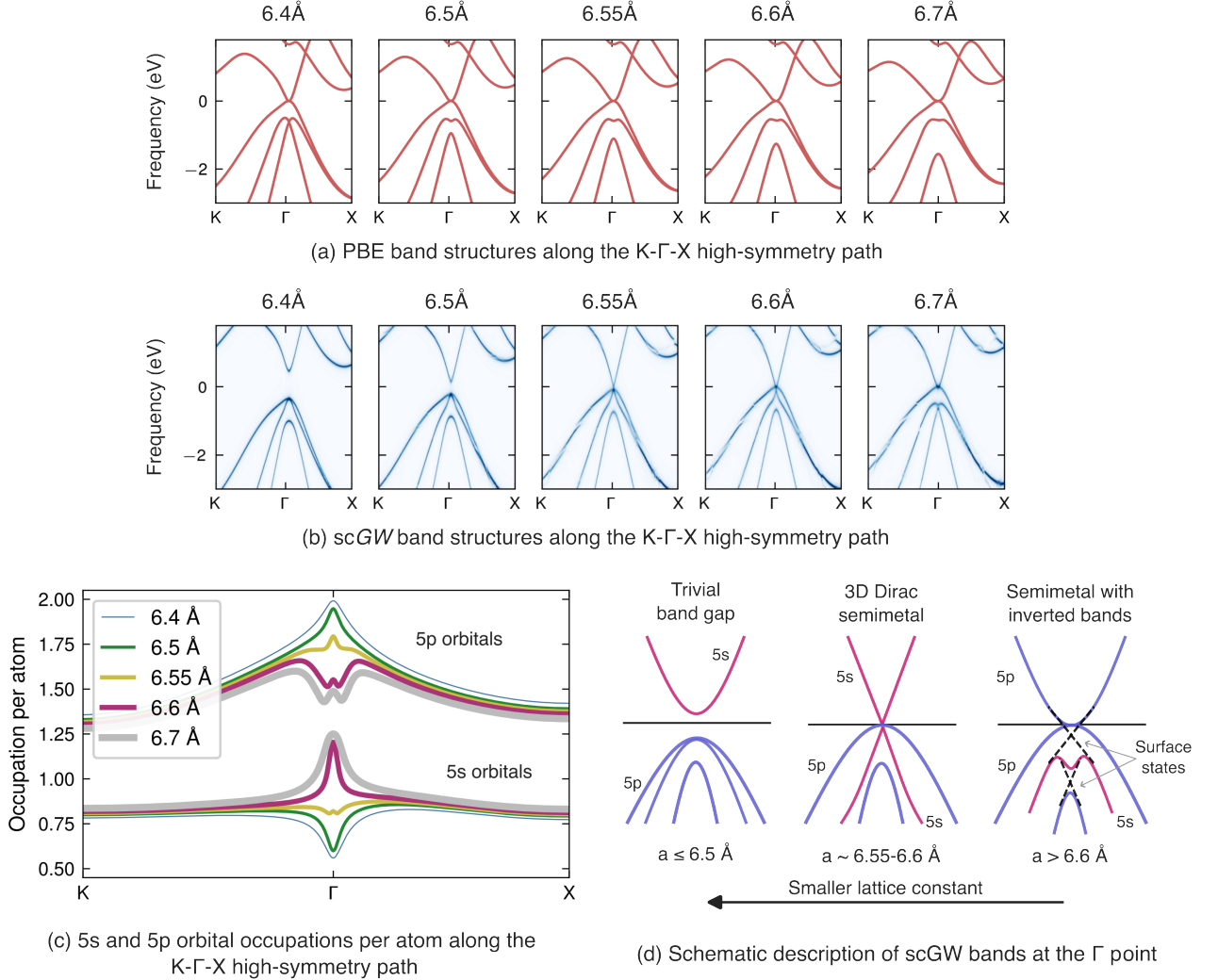


FIG. 2. **Influence of lattice parameter on the electronic structure of α -Sn.** (a) PBE and (b) scGW band structures along the K - Γ - X high-symmetry path for lattice constants ranging from 6.4 to 6.7 Å. (c) scGW orbital occupation trends for the 5s and 5p symmetrized atomic orbitals (SAOs). (d) Schematic illustration of the band evolution at the Γ point, highlighting the distinct electronic phases that emerge as the lattice parameter varies. In the native semimetallic phase of α -Sn, the double inversion between the 5s and 5p orbitals gives rise to two topological surface states [4].

shows good agreement with measured spectra. Fig. 3(a) shows that the effect of compression and elongation are rather opposite; while tensile strain results in a Dirac semimetal with the Dirac point along the Z - Γ path, the squeezed lattice exhibits avoided crossings with a twisted X-shaped valence band centered around Γ . The SAO occupation trends in Fig. 3(d) further show that the enhanced (reduced) occupation of the 5s (5p) orbitals near Γ does not change during [001] straining. These inverted occupation trends maintain the qualitative behavior of the unperturbed lattice, c.f., Fig. 1(c). Together with the 5s- and 5p-resolved spectral contributions in Fig. 3(b)-(c), these occupation trends confirm band inversion in both stretched and squeezed geometries, signifying non-trivial topology. Therefore, we con-

clude that the squeezed lattice forms a TI. Furthermore, in the compressed regime, the band structure forms a peculiar linear-dispersion caused by band-crossings nearly 0.2 eV below the Fermi level at Γ , potentially accessible through hole-doping. This feature arises from the re-ordering of the occupied 5s and 5p orbitals, which transforms the M-shaped dispersion of the unperturbed lattice (Fig. 2) into a twisted X-shape involving the upper valence bands, potentially restructuring the surface states. We emphasize that while the TI phase in the elongated geometry has been well characterized experimentally [10], the squeezed lattice remains largely unexplored.

We also examine the scGW band structures under compressive strain along the [111] crystallographic plane around $a = 6.7$ Å. For small strains, consistent with ex-

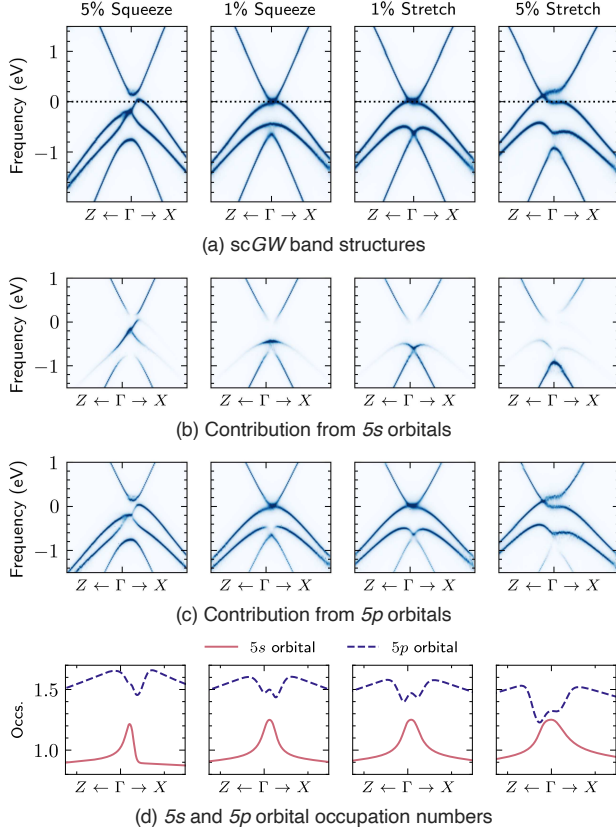


FIG. 3. **Effect of uniaxial strain along the [001] axis in bulk α -Sn:** (a) scGW band structure along the Z - Γ - X path; (b)-(c) spectral weight contribution from the $5s$ and $5p$ SAOs; and (d) corresponding orbital occupation trends. While the stretched lattice exhibits a Dirac semimetal, exemplified by a Dirac point along the Z - Γ path, the squeezed lattice develops into a topological insulator, visibly clearly under 5% strain. All results are shown near the Γ point, with $a = 6.7$, Å as the reference lattice parameter.

periments [3], the material exhibits signatures of 3D TDS induced by a marginal lowering of the conduction band below the Fermi level. For larger strains, a trivial band gap opens up with band structure similar to that for $a = 6.4$ Å. The results are presented in Fig. 2 of SI.

DISCUSSION

The vanishing band gap of α -Sn makes it extremely sensitive to external perturbations such as spin-orbit coupling and lattice distortions. The same feature also poses a formidable challenge for density functional theory. The relativistic, fully self-consistent GW method is ideally suited for such systems, as it naturally captures the delicate interplay among electron correlation, relativistic effects, and lattice distortions. For α -Sn, scGW offers several key advantages over conventional DFT. It corrects

the unphysical negative Γ -L band gap, yielding a zero or small gap around Γ for the lattice parameters considered. At the same time, scGW also captures the pronounced sensitivity of the electronic structure to external perturbations such as lattice distortions, an effect that underlies much of the material's scientific interest.

Using scGW, we uncover a previously unrecognized topological Dirac semimetal and a topological insulator phase featuring a Dirac-like band crossing just below the Fermi level. These phases emerge as the lattice is compressed uniformly or squeezed along the c -axis, respectively. We propose that the novel TI phase could be realized by growing α -Sn films on the [001] surface of a diamond- or zinc-blende-type substrate with a lattice constant larger than that of gray tin itself. Furthermore, the presence of linearly dispersing bands near the Fermi level opens the possibility of driving the TI phase into a 3D Dirac semimetal through p -doping.

More broadly, our results delineate a comprehensive topological phase diagram of bulk α -Sn, encompassing the experimentally familiar semimetal ground-state and two 3D TDS phases driven by compression along the [111] plane and tensile strain along the c axis. We attribute the remarkable topological tunability of α -Sn to the competition between spin-orbit coupling and the near-zero band-gap, modulated by lattice symmetry. This interplay allows numerous routes to manipulate the ordering of the Fermi level relative to the valence-shell $5s$ and $5p$ orbitals, thereby creating a rich spectrum of non-trivial electronic phases.

Conventionally, topological characterization relies on invariants computed from DFT or other mean-field eigenvalue spectra. However, these diagnostics lack a rigorous foundation when extended to post-DFT correlated methods. Here, we have introduced an alternative approach that combines orbital-resolved band and occupation dispersions, providing a robust framework for identifying topological phases beyond mean field theory. Our results illuminate the intricate electronic structure of α -Sn and open pathways for topological phase engineering in correlated materials.

METHODS

Self-consistent GW : We employ the fully self-consistent GW method for accurate and reliable investigation of the band structures of α -Sn. Based on Hedin's many-body perturbation theory [42], the GW self-energy consists of the first order Fock exchange and an infinite series of polarization diagrams, effectively capturing orbital-dependent screening of electron-electron interactions. As a result, the scGW method provides a systematic way for treating nonlocal and dynamical electronic correlation beyond DFT. Full self-consistency iteratively renormalizes both the Green's function and the

self-energy, thereby eliminating dependence on the initial DFT reference and making scGW a robust and predictive approach for electronic-structure calculations.

All calculations are initialized from DFT with the PBE functional, but the final scGW results are independent of this starting point. DFT results and Hamiltonian matrix elements are obtained using PySCF [69, 70], and the self-consistent GW iterations are performed with the GREEN package [54]. We employ all-electron Bloch Gaussian orbitals within the x2c-SVPA11 basis [71], which provides accurate results with a reduced number of contracted functions.

Our GW implementation uses the imaginary-time formalism with an inverse temperature of $\beta = 500 E_h^{-1}$ unless mentioned otherwise. The computed band structures show negligible changes when β is further increased, indicating convergence with respect to electronic temperature. Brillouin-zone integration is performed on a $6 \times 6 \times 6$ Monkhorst-Pack grid, and finite-size corrections are applied to treat the long-range Coulomb divergence in the scGW self-energy [54].

Spectral function: The GW calculations are carried out in a nonorthogonal atomic-orbital (AO) basis. Upon convergence, the Green's function is transformed to the symmetrized AO (SAO) basis [72] for post processing and analysis. The spectral function is defined as

$$A(\omega) = -\frac{1}{\pi} \Im G(\omega + i\eta), \quad (1)$$

and is obtained via analytic continuation of the Matsubara Green's function to the real frequency axis. We use the Nevanlinna approach [73] for continuation, though other schemes [74–76] can yield comparable results. The broadening parameter is set to $\eta = 0.0005 E_h^{-1}$ in all simulations, and artificially controls the width of spectral peaks.

Relativistic effects: Relativistic effects are included within the exact two-component (X2C) framework [46–50] for both DFT and scGW. In X2C, the four-component one-body Dirac–Coulomb Hamiltonian is block-diagonalized using a unitary transformation that decouples it into two blocks, namely the large- and small-component solutions. The large-component block serves as an effective one-body Hamiltonian for electrons, incorporating scalar-relativistic and spin-orbit effects. Relativistic corrections to the electron–electron interaction are neglected. The effective X2C Hamiltonian is constructed using PySCF. See Ref. [51] for further details on relativistic GW theory.

ACKNOWLEDGMENTS

This material is based upon work supported by the U.S. Department of Energy, Office of Science, Office of Advanced Scientific Computing Research and Office

of Basic Energy Sciences, Scientific Discovery through Advanced Computing (SciDAC) program under Award Number DE-SC0022198. This research used resources of the National Energy Research Scientific Computing Center, a DOE Office of Science User Facility supported by the Office of Science of the U.S. Department of Energy under Contract No. DE-AC02-05CH11231 using NERSC award BES-ERCAP0029462 and BES-ERCAP0024293. S.D. would like to acknowledge the Austrian Marshall Plan Foundation and TU Wien for enabling the research stay in Michigan. We also acknowledge helpful discussions with Kai Sun, Mariya Romanova, Aaron Engel, Christopher Palmstrøm and Vibin Abraham.

Author contributions: G.H. and S.D. performed most of the DFT and GW calculations. G.H. analyzed and interpreted the results and wrote the manuscript. E.G., V.V., and D.Z. conceived the study and contributed to the analysis and interpretation of the data.

-
- [1] S. Groves and W. Paul, Band Structure of Gray Tin, *Phys. Rev. Lett.* **11**, 194 (1963).
 - [2] C. A. Hoffman, J. R. Meyer, R. J. Wagner, F. J. Bartoli, M. A. Engelhardt, and H. Höchst, Three-band transport and cyclotron resonance in α -Sn and α Sn $_{1-x}$ Ge $_x$ grown by molecular-beam epitaxy, *Phys. Rev. B* **40**, 11693 (1989).
 - [3] C.-Z. Xu, Y.-H. Chan, Y. Chen, P. Chen, X. Wang, C. Dejoie, M.-H. Wong, J. A. Hlevyack, H. Ryu, H.-Y. Kee, N. Tamura, M.-Y. Chou, Z. Hussain, S.-K. Mo, and T.-C. Chiang, Elemental Topological Dirac Semimetal: α -Sn on InSb(111), *Phys. Rev. Lett.* **118**, 146402 (2017).
 - [4] V. A. Rogalev, T. Rauch, M. R. Scholz, F. Reis, L. Dudy, A. Fleszar, M.-A. Husanu, V. N. Strocov, J. Henk, I. Mertig, J. Schäfer, and R. Claessen, Double band inversion in α -Sn: Appearance of topological surface states and the role of orbital composition, *Phys. Rev. B* **95**, 161117 (2017).
 - [5] L. Gladczuk, L. Gladczuk, P. Dłuzewski, G. v. d. Laan, and T. Hesjedal, Study of Spin Pumping through α -Sn Thin Films, *physica status solidi (RRL) – Rapid Research Letters* **15**, 2100137 (2021).
 - [6] F. Binda, C. O. Avci, S. F. Alvarado, P. Noël, C.-H. Lambert, and P. Gambardella, Spin-orbit torques and magnetotransport properties of α -Sn and β -Sn heterostructures, *Phys. Rev. B* **103**, 224428 (2021).
 - [7] L. D. Anh, K. Takase, T. Chiba, Y. Kota, K. Takiguchi, and M. Tanaka, Elemental Topological Dirac Semimetal α -Sn with High Quantum Mobility, *Advanced Materials* **33**, 2104645 (2021).
 - [8] K. H. M. Chen, K. Y. Lin, S. W. Lien, S. W. Huang, C. K. Cheng, H. Y. Lin, C.-H. Hsu, T.-R. Chang, C.-M. Cheng, M. Hong, and J. Kwo, Thickness-dependent topological phase transition and Rashba-like preformed topological surface states of α -Sn(001) thin films on InSb(001), *Phys. Rev. B* **105**, 075109 (2022).
 - [9] Y. Zhang, V. Kalappattil, C. Liu, M. Mehraeen, S. S.-L. Zhang, J. Ding, U. Erugu, Z. Chen, J. Tian, K. Liu, J. Tang, and M. Wu, Large magnetoelectric resistance in

- the topological Dirac semimetal α -Sn, *Science Advances* **8**, eabo0052 (2022).
- [10] A. N. Engel, C. P. Dempsey, H. S. Inbar, J. T. Dong, S. Nishihaya, Y. Chang, A. V. Fedorov, M. Hashimoto, D. Lu, and C. J. Palmström, Growth and characterization of α -Sn thin films on In- and Sb-rich reconstructions of InSb(001), *Phys. Rev. Mater.* **8**, 044202 (2024).
 - [11] J. Polaczyński, G. Krizman, A. Kazakov, B. Turowski, J. B. Ortiz, R. Rudniewski, T. Wojciechowski, P. Dłużewski, M. Aleszkiewicz, W. Zaleszczyk, B. Kurowska, Z. Muhammad, M. Rosmus, N. Olszowska, L.-A. de Vaultier, Y. Guldner, T. Wojtowicz, and V. V. Volobuev, 3D topological semimetal phases of strained α -Sn on insulating substrate, *Materials Today* **75**, 135 (2024).
 - [12] M. S. Alam, A. Kazakov, M. Ahmad, R. Islam, F. Xue, and M. Matusiak, Quantum transport properties of the topological Dirac semimetal α -Sn, *Phys. Rev. B* **109**, 245135 (2024).
 - [13] B. Li, Y. Ding, J. Yao, X. Fan, G. Liu, Y.-B. Chen, J. Zhou, H. Lu, and Y.-F. Chen, Chiral anomaly in doped α -Sn films by Fermi level tuning, *Appl. Phys. Lett.* **126**, 093101 (2025).
 - [14] A. Barfuss, L. Dudy, M. R. Scholz, H. Roth, P. Höpfner, C. Blumenstein, G. Landolt, J. H. Dil, N. C. Plumb, M. Radovic, A. Bostwick, E. Rotenberg, A. Fleszar, G. Bihlmayer, D. Wortmann, G. Li, W. Hanke, R. Claessen, and J. Schäfer, Elemental Topological Insulator with Tunable Fermi Level: Strained α -Sn on InSb(001), *Phys. Rev. Lett.* **111**, 157205 (2013).
 - [15] J.-C. Rojas-Sánchez, S. Oyarzún, Y. Fu, A. Marty, C. Vergnaud, S. Gambarelli, L. Vila, M. Jamet, Y. Ohtsubo, A. Taleb-Ibrahimi, P. Le Fèvre, F. Bertran, N. Reyren, J.-M. George, and A. Fert, Spin to Charge Conversion at Room Temperature by Spin Pumping into a New Type of Topological Insulator: α -Sn Films, *Phys. Rev. Lett.* **116**, 096602 (2016).
 - [16] P. Borlido, A. W. Huran, M. A. L. Marques, and S. Botti, Structural prediction of stabilized atomically thin tin layers, *npj 2D Mater Appl* **3**, 21 (2019).
 - [17] N. Si, Q. Yao, Y. Jiang, H. Li, D. Zhou, Q. Ji, H. Huang, H. Li, and T. Niu, Recent Advances in Tin: From Two-Dimensional Quantum Spin Hall Insulator to Bulk Dirac Semimetal, *J. Phys. Chem. Lett.* **11**, 1317 (2020).
 - [18] O. Vail, A. Chang, S. Harrington, P. Folkes, P. Taylor, B. Nichols, C. Palmström, and G. de Coster, Gated Magnetotransport in α -Sn Thin Films on CdTe, *J. Electron. Mater.* **50**, 6329 (2021).
 - [19] M. J. A. Jardine, D. Dardzinski, M. Yu, A. Purkayastha, A.-H. Chen, Y.-H. Chang, A. Engel, V. N. Strocov, M. Hocevar, C. Palmstrøm, S. M. Frolov, and N. Marom, First-Principles Assessment of CdTe as a Tunnel Barrier at the α -Sn/InSb Interface, *ACS Appl. Mater. Interfaces* **15**, 16288 (2023).
 - [20] T. Bertoli, E. Stellino, F. Minati, C. Belloni, G. Tomasucci, E. Bosco, S. Battisti, L. Puppulin, D. Cristofori, V. Morandi, F. Rossi, D. Logoteta, A. Nucara, L. Barba, G. Campi, N. L. Saini, F. Palma, P. Riello, M. Back, and F. Irrera, Tuning Ultra-Narrow Direct Bandgap in α -Sn Nanocrystals: A CMOS-Compatible Approach for THz Applications, *Small* **n/a**, e09166 (2025).
 - [21] T. Brudevoll, D. S. Citrin, M. Cardona, and N. E. Christensen, Electronic structure of α -Sn and its dependence on hydrostatic strain, *Phys. Rev. B* **48**, 8629 (1993).
 - [22] S. Küfner, J. Furthmüller, L. Matthes, M. Fitzner, and F. Bechstedt, Structural and electronic properties of α -tin nanocrystals from first principles, *Phys. Rev. B* **87**, 235307 (2013).
 - [23] V. Vlček, G. Steinle-Neumann, L. Leppert, R. Armiento, and S. Kümmel, Improved ground-state electronic structure and optical dielectric constants with a semilocal exchange functional, *Phys. Rev. B* **91**, 035107 (2015).
 - [24] Z. Shi, X. Wang, C. Xu, P. Wang, Y. Liu, and T. C. Chiang, First-principles study of the topological surface states of α -Sn(111), *Physics Letters A* **384**, 126782 (2020).
 - [25] N. V. Smith, Inverse photoemission, *Rep. Prog. Phys.* **51**, 1227 (1988).
 - [26] F. Boschini, M. Zonno, and A. Damascelli, Time-resolved ARPES studies of quantum materials, *Rev. Mod. Phys.* **96**, 015003 (2024).
 - [27] B. Bradlyn, L. Elcoro, J. Cano, M. G. Vergniory, Z. Wang, C. Felser, M. I. Aroyo, and B. A. Bernevig, Topological quantum chemistry, *Nature* **547**, 298 (2017).
 - [28] J. Cano, B. Bradlyn, Z. Wang, L. Elcoro, M. G. Vergniory, C. Felser, M. I. Aroyo, and B. A. Bernevig, Building blocks of topological quantum chemistry: Elementary band representations, *Phys. Rev. B* **97**, 035139 (2018).
 - [29] J. Cano, B. Bradlyn, Z. Wang, L. Elcoro, M. G. Vergniory, C. Felser, M. I. Aroyo, and B. A. Bernevig, Topology of Disconnected Elementary Band Representations, *Phys. Rev. Lett.* **120**, 266401 (2018).
 - [30] B. A. Bernevig, T. L. Hughes, and S.-C. Zhang, Quantum Spin Hall Effect and Topological Phase Transition in HgTe Quantum Wells, *Science* **314**, 1757 (2006).
 - [31] L. Fu, C. L. Kane, and E. J. Mele, Topological Insulators in Three Dimensions, *Phys. Rev. Lett.* **98**, 106803 (2007).
 - [32] L. Fu and C. L. Kane, Topological insulators with inversion symmetry, *Phys. Rev. B* **76**, 045302 (2007).
 - [33] S. Murakami, Phase transition between the quantum spin Hall and insulator phases in 3D: emergence of a topological gapless phase, *New J. Phys.* **9**, 356 (2007).
 - [34] T. Zhang and S. Murakami, Predicting topological materials: symmetry-based indicator theories and beyond, *J. Phys. D: Appl. Phys.* **54**, 414002 (2021).
 - [35] J. Vidal, X. Zhang, L. Yu, J.-W. Luo, and A. Zunger, False-positive and false-negative assignments of topological insulators in density functional theory and hybrids, *Phys. Rev. B* **84**, 041109 (2011).
 - [36] A. K. Watkins, D. Johrendt, V. Vlcek, S. D. Wilson, and R. Seshadri, Fidelity and variability in the interlayer electronic structure of the kagome superconductor CsV₃Sb₅, *Phys. Rev. Mater.* **8**, 054204 (2024).
 - [37] D. Nabok, M. Tas, S. Kusaka, E. Durgun, C. Friedrich, G. Bihlmayer, S. Blügel, T. Hirahara, and I. Aguilera, Bulk and surface electronic structure of Bi₄Te₃ from GW calculations and photoemission experiments, *Phys. Rev. Mater.* **6**, 034204 (2022).
 - [38] I. Aguilera, C. Friedrich, G. Bihlmayer, and S. Blügel, GW study of topological insulators Bi₂Se₃, Bi₂Te₃, and Sb₂Te₃: Beyond the perturbative one-shot approach, *Phys. Rev. B* **88**, 045206 (2013).
 - [39] I. Aguilera, C. Friedrich, and S. Blügel, Electronic phase transitions of bismuth under strain from relativistic self-consistent GW calculations, *Phys. Rev. B* **91**, 125129 (2015).
 - [40] T. Förster, P. Krüger, and M. Rohlfing, GW calculations

- for Bi₂Te₃ and Sb₂Te₃ thin films: Electronic and topological properties, *Phys. Rev. B* **93**, 205442 (2016).
- [41] P. Aguado-Puente, S. Fahy, and M. Grüning, *GW* study of pressure-induced topological insulator transition in group-IV tellurides, *Phys. Rev. Res.* **2**, 043105 (2020).
- [42] L. Hedin, New Method for Calculating the One-Particle Green's Function with Application to the Electron-Gas Problem, *Phys. Rev.* **139**, A796 (1965).
- [43] F. Aryasetiawan and O. Gunnarsson, The *GW* method, *Rep. Prog. Phys.* **61**, 237 (1998).
- [44] L. Reining, The *GW* approximation: content, successes and limitations, *WIREs Computational Molecular Science* **8**, e1344 (2018).
- [45] D. Golze, M. Dvorak, and P. Rinke, The *GW* Compendium: A Practical Guide to Theoretical Photoemission Spectroscopy, *Front. Chem.* **0**, 10.3389/fchem.2019.00377 (2019).
- [46] W. Kutzelnigg and W. Liu, Quasirelativistic theory equivalent to fully relativistic theory, *J. Chem. Phys.* **123**, 241102 (2005).
- [47] W. Liu and W. Kutzelnigg, Quasirelativistic theory. II. Theory at matrix level, *J. Chem. Phys.* **126**, 114107 (2007).
- [48] Q. Sun, W. Liu, Y. Xiao, and L. Cheng, Exact two-component relativistic theory for nuclear magnetic resonance parameters, *J. Chem. Phys.* **131**, 081101 (2009).
- [49] T. Saue, Relativistic Hamiltonians for Chemistry: A Primer, *ChemPhysChem* **12**, 3077 (2011).
- [50] W. Liu, Essentials of relativistic quantum chemistry, *J. Chem. Phys.* **152**, 180901 (2020).
- [51] C.-N. Yeh, A. Shee, Q. Sun, E. Gull, and D. Zgid, Relativistic self-consistent *GW*: Exact two-component formalism with one-electron approximation for solids, *Phys. Rev. B* **106**, 085121 (2022).
- [52] C.-N. Yeh, S. Iskakov, D. Zgid, and E. Gull, Fully self-consistent finite-temperature *GW* in Gaussian Bloch orbitals for solids, *Phys. Rev. B* **106**, 235104 (2022).
- [53] V. Abraham, G. Harsha, and D. Zgid, Relativistic Fully Self-Consistent *GW* for Molecules: Total Energies and Ionization Potentials, *J. Chem. Theory Comput.* **20**, 4579 (2024).
- [54] S. Iskakov, C.-N. Yeh, P. Pokhilko, Y. Yu, L. Zhang, G. Harsha, V. Abraham, M. Wen, M. Wang, J. Adamski, T. Chen, E. Gull, and D. Zgid, Green/WeakCoupling: Implementation of fully self-consistent finite-temperature many-body perturbation theory for molecules and solids, *Computer Physics Communications* **306**, 109380 (2025).
- [55] G. Harsha, V. Abraham, M. Wen, and D. Zgid, Quasiparticle and fully self-consistent *GW* methods: An unbiased analysis using Gaussian orbitals, *Phys. Rev. B* **110**, 235146 (2024).
- [56] G. Harsha, V. Abraham, and D. Zgid, Challenges with relativistic *GW* calculations in solids and molecules, *Faraday Discuss.* **254**, 216 (2024).
- [57] J. Thewlis and A. R. Davey, Thermal Expansion of Grey Tin, *Nature* **174**, 1011 (1954).
- [58] R. F. C. Farrow, D. S. Robertson, G. M. Williams, A. G. Cullis, G. R. Jones, I. M. Young, and P. N. J. Dennis, The growth of metastable, heteroepitaxial films of α -Sn by metal beam epitaxy, *Journal of Crystal Growth* **54**, 507 (1981).
- [59] J. P. Perdew, K. Burke, and M. Ernzerhof, Generalized Gradient Approximation Made Simple, *Phys. Rev. Lett.* **77**, 3865 (1996).
- [60] S. M. Young, S. Zaheer, J. C. Y. Teo, C. L. Kane, E. J. Mele, and A. M. Rappe, Dirac Semimetal in Three Dimensions, *Phys. Rev. Lett.* **108**, 140405 (2012).
- [61] Z. Wang, Y. Sun, X.-Q. Chen, C. Franchini, G. Xu, H. Weng, X. Dai, and Z. Fang, Dirac semimetal and topological phase transitions in A₃Bi (A = Na, K, Rb), *Phys. Rev. B* **85**, 195320 (2012).
- [62] B.-J. Yang and N. Nagaosa, Classification of stable three-dimensional Dirac semimetals with nontrivial topology, *Nat Commun* **5**, 4898 (2014).
- [63] Q. Wu, S. Zhang, H.-F. Song, M. Troyer, and A. A. Soluyanov, Wanniertools : An open-source software package for novel topological materials, *Computer Physics Communications* **224**, 405 (2018).
- [64] G. Pizzi, V. Vitale, R. Arita, S. Blügel, F. Freimuth, G. Géranton, M. Gibertini, D. Gresch, C. Johnson, T. Koretsune, J. Ibañez-Azpiroz, H. Lee, J.-M. Lihm, D. Marchand, A. Marrazzo, Y. Mokrousov, J. I. Mustafa, Y. Nohara, Y. Nomura, L. Paulatto, S. Poncé, T. Ponweiser, J. Qiao, F. Thöle, S. S. Tsirkin, M. Wierzbowska, N. Marzari, D. Vanderbilt, I. Souza, A. A. Mostofi, and J. R. Yates, Wannier90 as a community code: new features and applications, *Journal of Physics: Condensed Matter* **32**, 165902 (2020).
- [65] A. Lopez, C. A. Melton, J. Ahn, B. M. Rubenstein, and J. T. Krogel, Identifying Band Inversions in Topological Materials Using Diffusion Monte Carlo, *J. Chem. Theory Comput.* **10.1021/acs.jctc.5c00838** (2025).
- [66] V. Gurarie, Single-particle Green's functions and interacting topological insulators, *Phys. Rev. B* **83**, 085426 (2011).
- [67] A. M. Essin and V. Gurarie, Bulk-boundary correspondence of topological insulators from their Green's functions, *Phys. Rev. B* **84**, 125132 (2011).
- [68] T. Misawa and Y. Yamaji, Zeros of Green functions in topological insulators, *Phys. Rev. Res.* **4**, 023177 (2022).
- [69] Q. Sun, T. C. Berkelbach, N. S. Blunt, G. H. Booth, S. Guo, Z. Li, J. Liu, J. D. McClain, E. R. Sayfutyarova, S. Sharma, S. Wouters, and G. K.-L. Chan, PySCF: the Python-based simulations of chemistry framework, *WIREs Computational Molecular Science* **8**, e1340 (2018).
- [70] Q. Sun, X. Zhang, S. Banerjee, P. Bao, M. Barbry, N. S. Blunt, N. A. Bogdanov, G. H. Booth, J. Chen, Z.-H. Cui, J. J. Eriksen, Y. Gao, S. Guo, J. Hermann, M. R. Hermes, K. Koh, P. Koval, S. Lehtola, Z. Li, J. Liu, N. Mardirossian, J. D. McClain, M. Motta, B. Mussard, H. Q. Pham, A. Pulkin, W. Purwanto, P. J. Robinson, E. Ronca, E. R. Sayfutyarova, M. Scheurer, H. F. Schurkus, J. E. T. Smith, C. Sun, S.-N. Sun, S. Upadhyay, L. K. Wagner, X. Wang, A. White, J. D. Whitfield, M. J. Williamson, S. Wouters, J. Yang, J. M. Yu, T. Zhu, T. C. Berkelbach, S. Sharma, A. Y. Sokolov, and G. K.-L. Chan, Recent developments in the PySCF program package, *J. Chem. Phys.* **153**, 024109 (2020).
- [71] P. Pollak and F. Weigend, Segmented Contracted Error-Consistent Basis Sets of Double- and Triple- ζ Valence Quality for One- and Two-Component Relativistic All-Electron Calculations, *J. Chem. Theory Comput.* **13**, 3696 (2017).
- [72] P.-O. Löwdin, On the Nonorthogonality Problem*, in *Advances in Quantum Chemistry*, Vol. 5, edited by P.-O. Löwdin (Academic Press, 1970) pp. 185–199.
- [73] J. Fei, C.-N. Yeh, and E. Gull, Nevanlinna Analytical

- Continuation, [Phys. Rev. Lett. **126**, 056402 \(2021\)](#).
- [74] J. Fei, C.-N. Yeh, D. Zgid, and E. Gull, Analytical continuation of matrix-valued functions: Carathéodory formalism, [Phys. Rev. B **104**, 165111 \(2021\)](#).
- [75] Z. Huang, E. Gull, and L. Lin, Robust analytic continuation of Green's functions via projection, pole estimation, and semidefinite relaxation, [Phys. Rev. B **107**, 075151 \(2023\)](#).
- [76] L. Zhang, Y. Yu, and E. Gull, Minimal pole representation and analytic continuation of matrix-valued correlation functions, [Phys. Rev. B **110**, 235131 \(2024\)](#).

Supplemental Information for “Discovering topological phases in gray-Tin”

Gaurav Harsha,¹ Selina Dirnböck,^{2,3} Emanuel Gull,^{2,4} Vojtěch Vlček,^{5,6} and Dominika Zgid^{1,2,4}

¹*Department of Chemistry, University of Michigan, Ann Arbor, MI 48109, USA*

²*Department of Physics, University of Michigan, Ann Arbor, MI 48109, USA*

³*Institute of Solid State Physics, TU Wien, 1040 Vienna, Austria*

⁴*Department of Physics, University of Warsaw, Pasteura 1, 02-093 Warsaw, Poland*

⁵*Department of Chemistry and Biochemistry, University of California, Santa Barbara, CA 93106, USA*

⁶*Department of Materials, University of California, Santa Barbara, CA 93106, USA*

(Dated: December 1, 2025)

I. ORBITAL RESOLVED BAND STRUCTURES

Figure 2 in the main manuscript presents the fully self-consistent GW (sc GW) band structure and topological character of uniformly compressed α -Sn for several lattice parameters. The analysis is based on momentum-resolved occupations of symmetrized atomic orbitals (SAOs) along the K - Γ - X high-symmetry path. Here, we provide additional insight by comparing the orbital-resolved spectra of the valence $5s$ and $5p$ SAOs across different lattice constants. To complement the results in the main text showing a transition from an inverted semimetal to a trivial insulator, Fig. 1 displays the corresponding orbital-resolved spectra, highlighting the spectral weight from $5s$ and $5p$ SAOs. A clear semimetal-to-insulator transition is observed, mediated by Dirac-like crossings around $a \simeq 6.55$ Å that originate primarily from the $5s$ bands.

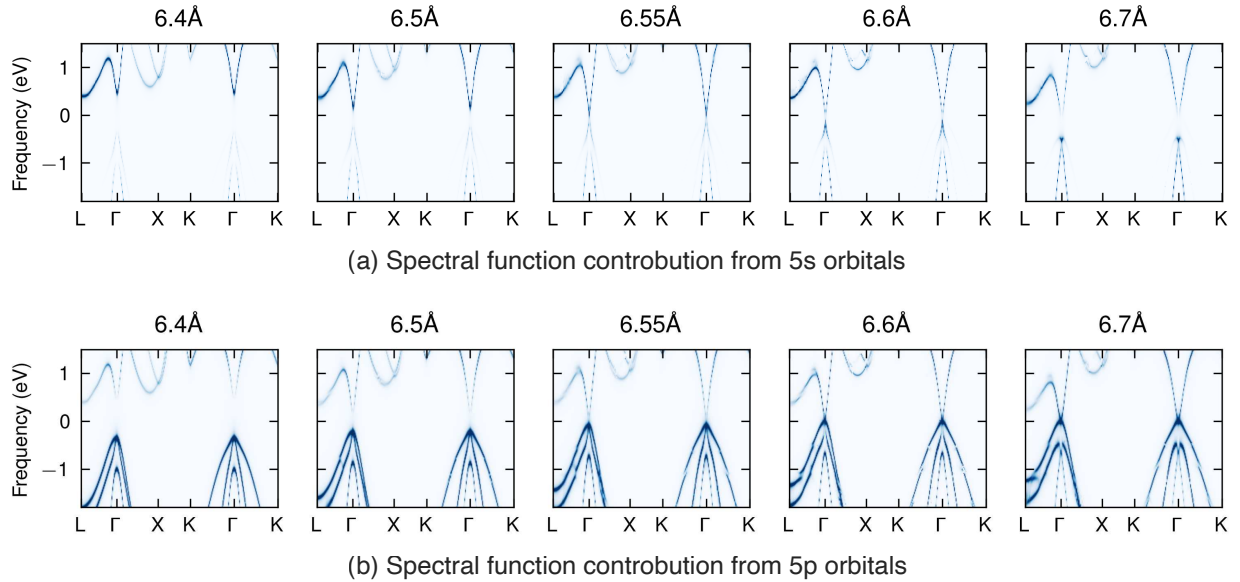


FIG. 1. **Orbital resolved band structures of α -Sn:** Contribution from (a) $5s$, and (b) $5p$ symmetrized atomic orbitals to the band structures of α -Sn for various lattice constants.

II. ORBITAL RESOLVED BAND STRUCTURES FOR IN-PLANE STRAIN ALONG [111]

Figure 2 shows the sc GW band structures of α -Sn under compression along the $[111]$ plane, using $a = 6.7$ Å as the reference geometry. By comparing the contributions from $5s$ and $5p$ orbitals from panels (b) and (c), we see that that especially for 2% compression, the $5s$ -character conduction bands are nearly linear around Γ at the Fermi level. However, at Γ , both conduction and valence bands are dominated by $5p$ character, and a marginal lowering of the conduction band below the Fermi level leads to the formation of a Dirac semimetal. Further compression opens the band gap, and destroys the band inversion, resulting in valence and conduction bands comprised purely of $5p$ and $5s$ characters, respectively. This is also visible in orbital-resolved occupation trends shown in panel (d), as well as by

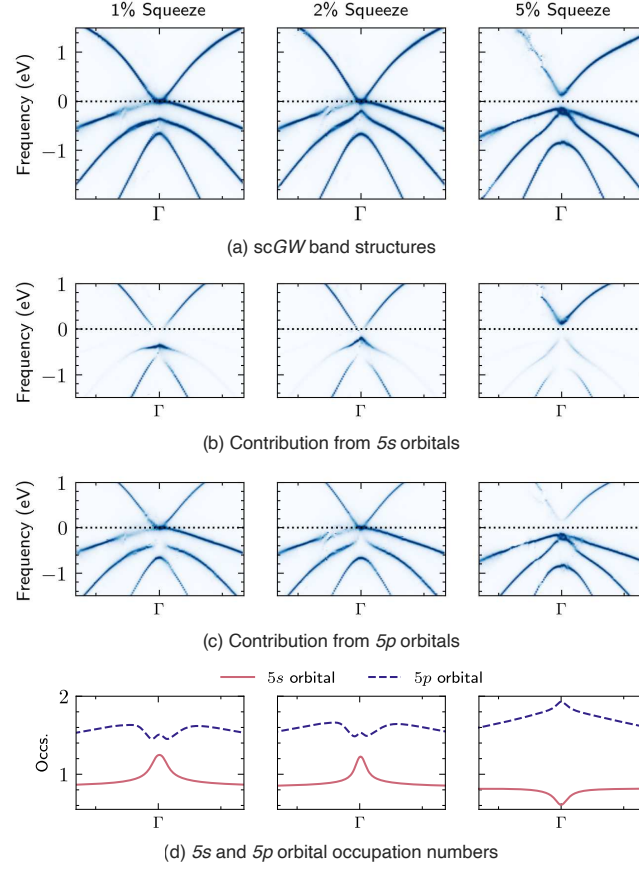


FIG. 2. **Effect of in-plane compressive strain along [111] in bulk α -Sn:** (a) scGW band structure along the P - Γ - X path; (b)-(c) spectral weight contribution from the 5s and 5p SAOs; and (d) corresponding orbital occupation trends. Compressive strain first introduces a marginal lowering of the conduction bands below the Fermi level, before eventually opening a trivial band-gap at Γ .

comparing the 5% strained geometry with results for $a = 6.4 \text{ \AA}$ in Fig. 1. Additionally, compressive strain along [111] destroys the M-shape which is related to topological surface states in α -Sn, as noted in the main manuscript.

We note that a clear and obvious observation of Dirac band crossing in the [111] strained α -Sn is nearly impossible beyond mean-field or tight-binding models, as the band crossing occurs within 100 meV around the Fermi level. However, by decomposing the orbital contributions, we can amplify the signatures of such features.

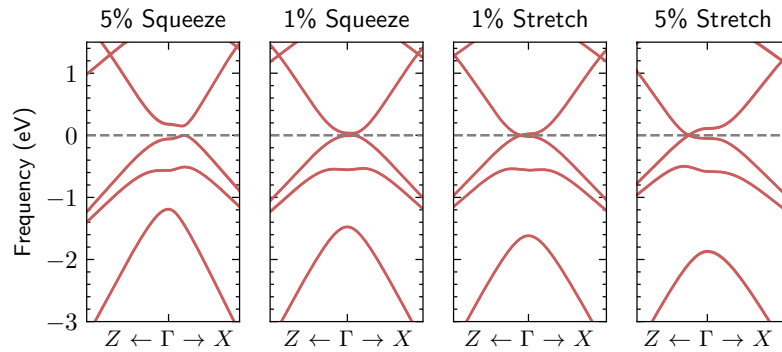


FIG. 3. **Effect of [001] straining:** PBE bands for various degrees of compressive and tensile strain along the c -axis in α -Sn. The results serve as a reference to compare the scGW band structures in the main manuscript.

III. PBE BAND STRUCTURES FOR UNIAXIAL STRAIN ALONG c -AXIS

In the main manuscript, we analyze the effects of uniaxial straining along the c axis, i.e., perpendicular to [001] plane, using the *scGW* framework. We show that while a tensile strain induces a topological Dirac semimetal phase, compressive strain results in a topological insulator (TI). In addition to a non-trivial band gap around Γ , this TI phase exhibits a linearly-dispersing band crossing nearly 200 meV below the Fermi level.

Here, we show the results obtained from density functional theory to reiterate the efficacy of *scGW*. Figure 3 shows the PBE bands for the various c -axis strained α -Sn lattices. For tensile strained configurations, PBE predicts a Dirac point along the Z - Γ path, qualitatively consistent with *scGW*. For the squeezed configurations, while PBE predicts a band gap opening, it completely misses the peculiar band crossing just below the Fermi level, which is observed in the *GW* results. These results highlight the qualitative and quantitative prowess of *scGW* over DFT.